promising. Since abnormalities on fMRI and FDG-PET reflect different aspects of tumor metabolism, proliferation of new blood vessels versus elevated glucose metabolism, the techniques are likely to be complementary.

CONCLUSION

This report demonstrates that the finding of intense hypermetabolism by FDG-PET is not pathognomonic for recurrence in patients with brain tumors treated with radiation. However, despite this very infrequent pattern, the procedure remains an extremely important tool for the metabolic evaluation of brain tumors.

REFERENCES

1. Di Chiro G, Oldfield E, Wright DC, et al. Cerebral necrosis after radiotherapy and/or intra-arterial chemotherapy for brain tumors: PET and neuropathologic studies. *Am J Roentgenol* 1988;150:189–197.
2. Valk PE, Budinger TF, Levin VA, Silver P, Gutin PH, Doyle WK. PET of malignant cerebral tumors after interstitial brachytherapy. Demonstration of metabolic activity and correlation with clinical outcome. *J Neurosurg* 1988;69:830–838.
3. Doyle WK, Budinger TF, Valk PE, Levin VA, Gutin PH. Differentiation of cerebral radiation necrosis from tumor recurrence by [^{18}F]FDG and ^{82}Rb PET. *J Comput Assist Tomogr* 1987;11:563–570.
4. Martins AN, Johnston JS, Henry JM, Stoffel TJ, Di Chiro G. Delayed radiation necrosis of the brain. *J Neurosurg* 1977;47:336–345.
5. Dooms GC, Hecht S, Brant-Zawadzki M, Berthiaume Y, Norman D, Newton TH. Brain radiation lesions: MR imaging. *Radiology* 1986;158:149–155.
6. Buchpiguel CA, Alavi JB, Alavi A, Kenyon LC. PET versus SPECT in distinguishing radiation necrosis from tumor recurrence in the brain. *J Nucl Med* 1995;36:159–164.
7. Rota Kops E, Herzog H, Schmid A, Holte S, Feinendegen LE. Performance characteristics of an eight-ring whole-body PET scanner. *J Comput Assist Tomogr* 1990;14:437–445.
8. Alpert NM, Berdichevsky D, Levin Z, Morris ED, Fischman AJ. Improved methods for image registration. *J Neuro Image* 1996;3:10–18.
9. Jones HA, Clark RJ, Rhodes CG, Schofield JB, Krausz T, Haslett C. Positron emission tomography of ^{18}FDG uptake in localized pulmonary inflammation. *Acta Radiol Suppl* 1991;376:148.
10. Yamada S, Kubota K, Kubota R, Ido T, Tamahashi N. High accumulation of fluorine-18-fluorodeoxyglucose in turpentine-induced inflammatory tissue. *J Nucl Med* 1995;36:1301–1306.
11. Larson SM. Cancer or inflammation? A holy grail for nuclear medicine. *J Nucl Med* 1994;35:1653–1655.
12. Palmer WE, Rosenthal DI, Schoenberg OI, et al. Quantification of inflammation in the wrist with gadolinium-enhanced MR imaging and PET with ^{18}F-2-fluoro-2-deoxy-D-glucose. *Radiology* 1995;196:647–655.
13. Jones HA, Clark RJ, Rhodes CG, Schofield JB, Krausz T, Haslett C. In vivo measurement of neutrophil activity in experimental lung inflammation. *Am J Respir Crit Care Med* 1994;149:1635–1639.
14. Tahara T, Ichiya Y, Kuwabara Y, et al. High ^{18}F-fluorodeoxyglucose uptake in abdominal abscesses: a PET study. *J Comput Assist Tomogr* 1989;13:829–831.
15. Fukuda H, Yoshioka S, Watanuki S, et al. Experimental study for cancer diagnosis with ^{18}F-FDG: differential diagnosis of inflammation from malignant tumor. *Kaku Igaku* 1983;20:1189–1192.
16. Sasaki M, Ichiya Y, Kuwabara Y, et al. Ringlike uptake of ^{18}F-FDG in brain abscess: a PET study. *J Comput Assist Tomogr* 1990;14:486–487.
17. Meyer MA, Frey KA, Schwaiger M. Discordance between ^{18}F-fluorodeoxyglucose uptake and contrast enhancement in a brain abscess. *Clin Nucl Med* 1993;18:682–684.
18. Schwartz RB, Carvalho PA, Alexander E, et al. Radiation necrosis versus high-grade recurrent glioma: differentiation by using dual-isotope SPECT with ^{201}TI and ^{99m}Tc-HMPAO. *AJNR* 1991;12:1187–1192.
19. Alexander E, Loeffler JS, Schwartz RB, et al. Thallium-201 technetium-99m-HMPAO SPECT imaging for guiding stereotactic craniotomies in heavily irradiated malignant glioma patients. *Acta Neurochir (Wien)* 1993;122:215–217.
20. Moody EB, Hodes JE, Walsh JW, Thornsberry S. Thallium-avid cerebral radiation necrosis. *Clin Nucl Med* 1994;19:611–613.

Comparative PET Imaging of Experimental Tumors with Bromine-76-Labeled Antibodies, Fluorine-18-Fluorodeoxyglucose and Carbon-11-Methionine

Anna Lövqvist, Anders Sundin, Amilcar Roberto, Håkan Ahlström, Jörgen Carlsson and Hans Lundqvist

Biomedical Radiation Sciences, Departments of Diagnostic Radiology and Pharmaceutical Biosciences, Uppsala University, and Uppsala University PET Centre, Akademiska Sjukhuset, Uppsala, Sweden

The potential of a ^{76}Br-labeled anti-carcinoembryonic antigen monoclonal antibody (MAb), 38S1, as a tumor-imaging agent for PET was investigated in a comparative experimental study with [^{18}F]fluorodeoxyglucose ([^{18}F]FDG) and L-[methyl-^{11}C]methionine ([^{11}C]Met). **Methods:** The three radiotracers were administered to nude rats carrying subcutaneous xenografts or liver metastases from a human colonic carcinoma. Tracer biodistribution was evaluated by PET imaging and radioactivity measurement of dissected tissues and also by whole-body autoradiography for subcutaneous xenografts. **Results:** For PET imaging of subcutaneous tumors, ^{76}Br-38S1 proved superior to the other radiotracers. Tumor-to-tissue ratios were, except for the tumor-to-blood ratio, generally higher for ^{76}Br-labeled MAb than for [^{18}F]FDG and [^{11}C]Met. Liver metastases were imaged with PET using both ^{76}Br-38S1 and [^{18}F]FDG, and the metastases-to-liver ratios of dissected samples were not significantly different for the two radiotracers. **Conclusion:** The tumor-imaging capacity of ^{76}Br-labeled MAb 38S1 was superior to [^{18}F]FDG and [^{11}C]Met in the subcutaneous tumor model, whereas ^{76}Br-38S1 and [^{18}F[FDG were equally successful for the identification of liver metastases.

Received Feb. 28, 1996; revision accepted Sep. 19, 1996.

For correspondence or reprints contact: Anna Lövqvist, MSc, Biomedical Radiation Sciences, Uppsala University, Box 535, S-751 21 Uppsala, Sweden.

Key Words: bromine-76; PET; monoclonal antibodies; fluorine-18-FDG; carbon-11-methionine

J Nucl Med 1997; 38:1029–1035

Several diagnostic problems involving the imaging and characterization of malignant tissues might benefit from the advantages of PET. The quantitative and temporal data obtained with PET can give valuable information about the functional and metabolic status of a lesion. The most commonly used agent for tumor imaging by PET is [^{18}F]fluorodeoxyglucose ([^{18}F]FDG) because the increased metabolic activity of many malignant tumors is reflected by a higher uptake of [^{18}F]FDG than in most normal tissues (*1*). Fluorine-18-FDG-PET has been useful for the detection, staging and treatment monitoring of a variety of malignant diseases (*2*). In the case of colorectal cancer, studies have demonstrated the usefulness of [^{18}F]FDG-PET in imaging of metastatic and recurrent disease (*3–6*). Amino acids as tumor-imaging agents have also proven valuable by taking advantage of an increased membrane transport or protein synthesis rate in the tumor. For instance, L-[methyl-^{11}C]methionine ([^{11}C]Met) has been successfully applied for imaging of tumors in the brain (*7,8*) and in the lung (*9,10*).

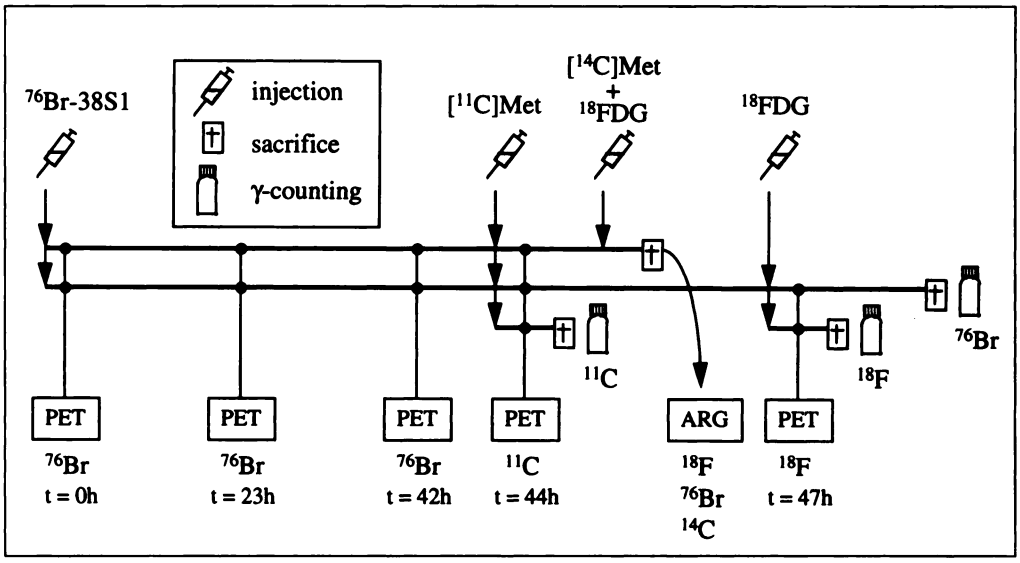

FIGURE 1. Overview of the experimental procedure used for studying the kinetics and distribution of ^{76}Br-38S1, [^{18}F]FDG and [^{11}C]Met/[^{14}C]Met in nude rats carrying subcutaneous LS174T tumors. Each horizontal line represents two animals. Biodistribution was evaluated by PET, whole-body autoradiography (ARG) and gamma counting of dissected tissues. A similar protocol was applied in the case of rats carrying liver metastases, but the distribution of radiolabeled Met was not investigated in this model and ARG was excluded.

In radioimmunodetection, tumor uptake of radiotracer does not rely primarily on the metabolic status of a lesion but on the specific binding of radiolabeled monoclonal antibodies (MAbs) to tumor antigens. Therefore, MAbs could serve as more specific tools for tumor detection and characterization, provided that the expression of these antigens is mainly restricted to tumor cells. The clinical application of MAbs as PET tracers has so far been limited to a small number of studies (*11–13*), although numerous immunoscintigraphy trials using gamma camera or SPECT have been performed (*14,15*). Much attention has been focused on recurrent colorectal carcinoma, where immunoscintigraphy has been shown to be a useful complement to conventional radiological methods (*16–19*).

In previous studies, the anti-carcinoembryonic antigen (CEA) MAb 38S1 was labeled with the positron-emitting nuclide ^{76}Br ($T_{1/2}$, 16 hr) (*20*), and the distribution kinetics were evaluated in a xenograft model (*21*). The aim of the present investigation was to compare the biodistribution and tumor-imaging capability of ^{76}Br-labeled MAbs with [^{18}F]FDG and [^{11}C]Met in nude rats carrying either subcutaneous tumors or liver metastases from human colorectal carcinoma.

MATERIALS AND METHODS

Radiotracers

Bromine-76 was produced at the Gustaf Werner Cyclotron (The Svedberg Laboratory, Uppsala, Sweden) using the reactions ^{nat}Br(p, xn)^{76}Kr, ^{76}Kr($T_{1/2}$, 15 hr) → ^{76}Br($T_{1/2}$, 16 hr) (*22*). MAb 38S1, kindly donated by Pharmacia (Uppsala, Sweden) is a mouse anti-CEA antibody of the immunoglobulin G1κ isotype (*23*). A partially purified preparation of bromoperoxidase was used (Sigma Chemical Co., St. Louis, MO).

Bromine-76-MAb 38S1. MAb 38S1 (100 μg) was mixed with 0.2 units of bromoperoxidase and 60–80 MBq of ^{76}Br in 50 m*M* sodium phosphate buffer (pH 7.0) (*20*). After the addition of H_2O_2 to a concentration of 80–160 μ*M* and a total volume of 200 μl, the reaction was allowed to continue for 40–60 min at 0°C. Bromine-76–38S1 was separated from bromoperoxidase and low-molecular weight components using a size-exclusion FPLC column coupled to an HPLC system (Beckman 126 pump and 166 UV detector, βflow detector; Pharmacia FRAC-100 fraction collector). After elution in 50 m*M* phosphate-buffered saline (PBS) (pH 7.3), the amount of protein-bound radioactivity in the final ^{76}Br-38S1 preparation was determined by 10% trichloroacetic acid precipitation. Preservation of immunoreactivity was tested in a single point binding assay in which radiolabeled 38S1 was incubated overnight with an excess of CEA covalently coupled to paper disks.

Fluorine-18-FDG. Fluorine-18-FDG in sterile water was prepared with >98% radiochemical purity using a PETtrace FDG Microlab System (General Electric Medical Systems, Uppsala, Sweden) (*24*).

L-[methyl-Carbon-11]Met. Carbon-11-Met in sterile PBS with >95% radiochemical purity was prepared as previously described (*25*).

L-[methyl-Carbon-14]Met. Carbon-14-Met in 70% ethanol was purchased from DuPont Scandinavia AB/New England Nuclear Research Products (Stockholm, Sweden) at a specific activity of 1.5–2.0 GBq/mole and diluted in sterile PBS.

Tumor Models

The CEA-producing human colorectal carcinoma cell line LS174T was used for tumor inoculation in nude rats (Rowett nu/nu, 5–8 wk old). For anesthesia, Ekvisitin (4.25 g of chloral hydrate and 0.97 g of pentobarbital per 100 ml) or Inactin® was given intraperitonially.

Subcutaneous Tumors. LS174T cells (5×10^6) were injected subcutaneously in the right hind leg and left flank of eight nude rats and allowed to grow for 3 wk. At the time of experiment, tumors weighed 0.3–1.4 g.

Liver Metastases. The surgical procedure for induction of experimental hepatic metastases has been described in detail elsewhere (*26*). Five rats were injected with 5×10^6 LS174T cells into a peripheral branch of the superior mesenteric vein 6 wk before tracer administration. At the time of the experiment, all rats carried one or several liver metastases, weighing up to 1.3 g.

Biodistribution Experiment

An overview of the experimental procedure is shown in Figure 1.

Tracer Administration. Bromine-76–38S1 (2–4 MBq) or [^{18}F]FDG (10–20 MBq) was injected into the left femoral vein, cannulated with a plastic catheter through a groin incision, in rats carrying subcutaneous tumors or liver metastases. Carbon-11-Met (10 MBq) or [^{14}C]Met (200 kBq) was injected only in rats carrying subcutaneous tumors. Some rats received more than one radiotracer (Fig. 1), but the experiment was designed to allow selective study of each radiotracer with only minimal influence from other radionuclides.

Pharmacokinetics and PET Imaging. For analysis of blood clearance rate, blood samples were drawn from a tail vein at 0.5, 1,

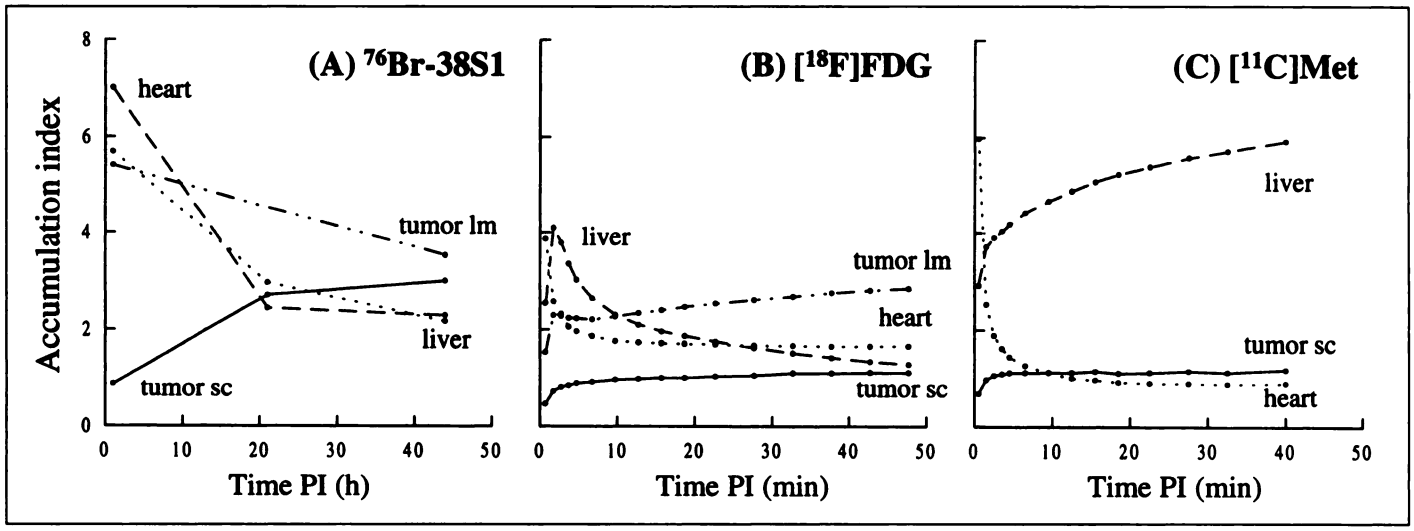

FIGURE 2. Kinetics of ^{76}Br-38S1 (A), [^{18}F]FDG (B) and [^{11}C]Met (C) evaluated by PET imaging (n = 4–6). tumor sc = subcutaneous tumors; tumor lm = liver metastases. Error bars were omitted for clarity.

2, 7, 15, 22, 40 and 49 hr after injection of ^{76}Br-38S1. For PET imaging, the rats were placed prone in a plastic multicompartment holder, which allowed simultaneous examination of up to seven rats. The Scanditronics GE 2048 PET-scanner (Scanditronics AB, Uppsala, Sweden) allowed examination of an axial 10-cm region divided into 15 slices. Transmission scans, corrected for previously injected radioactivity when necessary, were used for attenuation correction. Imaging of ^{76}Br-38S1 distribution in four rats was performed at 0, 21 and 42 hr postinjection in the case of subcutaneous tumors and at 0 and 48 hr postinjection in two rats in the case of liver metastasis. On each occasion, emission data was collected during five serial 15-min frames, and summation images were made of all frames. Standard PET protocols were used for dynamic imaging of [^{18}F]FDG for 50 min (four rats carrying subcutaneous tumors and five rats with liver metastasis) and for imaging of [^{11}C]Met for 45 min (six rats carrying subcutaneous tumors). In these cases, summation images were created by adding all frames obtained after 30 min postinjection. In the summation PET images, radionuclide concentration in subcutaneous tumors, liver metastasis, heart and kidney was measured in 0.8-cm^2 circular regions of interest (ROIs). Radionuclide concentration in normal liver was measured only in rats carrying subcutaneous tumors by applying 3-cm^2 circular ROIs. Standard uptake values (SUVs) were calculated as (tissue radioactivity/ml of tissue)/(injected radioactivity/g of body weight). Assuming a tissue density of 1 g/ml, SUV corresponds to the accumulation index (AI) (see below).

Whole-Body Autoradiography. Whole-body autoradiography of two animals carrying subcutaneous tumors was performed according to Ullberg et al. (*27*). Both rats had been injected with ^{76}Br-38S1 47 hr before kill and with a mixture of [^{18}F]FDG and [^{14}C]Met 1 hr before kill. Animal bodies were embedded in an aqueous gel of carboxymethyl cellulose and frozen by immersion in a mixture of solid carbon dioxide and n-hexane (−78°C). Coronal sections, 20-μm-thick, were placed on film and stored at −20°C or rapidly dried and apposed to phosphorimaging plates during exposition. At certain time intervals, the sections were applied on new films or plates to obtain autoradiograms with minimal influence (<10% of total radioactivity) of the other radionuclides present. In the ^{76}Br and ^{18}F autoradiograms (plates), the counts per pixel in ROIs corresponding to tumors and selected normal tissues were analyzed with a PhosphorImager® (Molecular Dynamics, Sunnyvale, CA). The density pattern in ^{14}C autoradiograms (film) was evaluated using an image analyzer and a public domain image processing program (NIH Image). ROIs surrounding the whole organ were used except for tumors, intestines and blood vessels, where the tissue parts exhibiting the highest uptake were measured. A tumor-to-normal tissue ratio was calculated for each tumor and section.

Tissue Uptake. For each radionuclide and tumor model, two rats were killed by exsanguination under anesthesia at 48–50 hr postinjection for ^{76}Br-38S1 and 1 hr postinjection for [^{18}F]FDG and [^{11}C]Met. Blood, urine, dissected subcutaneous tumors, liver metastases and pieces of normal tissues were weighed and measured for radioactivity in a well scintillation NaI(Tl) detector. From decay-corrected radionuclide uptake data, the AI was calculated, corresponding to (radioactivity/g of tissue)/(injected radioactivity/g of body weight). A tumor-to-normal tissue ratio was calculated for each tumor and animal.

RESULTS

Bromine-76-38S1 Preparation

The overall radiochemical yield of ^{76}Br labeling and purification of ^{76}Br-38S1 was 29 ± 3%, in a total preparation time of 60–90 min. The final preparation contained 19–22 MBq of ^{76}Br-38S1 at a specific activity of approximately 0.2 MBq/μg. More than 97% of the ^{76}Br activity was protein bound, according to trichloroacetic acid precipitation. The immunoreactivity of ^{76}Br-38S1 was 70%–75%.

Pharmacokinetics

Blood Measurements. Thirty minutes after the injection of ^{76}Br-38S1, the AI in blood was 16 ± 4 (mean ± s.d.). After a decrease to half of the initial value in about 7 hr, blood clearance was slower, reaching 2.8 ± 0.6 after 2 days.

PET Measurements. During the first hour after ^{76}Br-38S1 injection, a high uptake of ^{76}Br activity could be observed in heart and normal liver, both containing a large blood pool (Fig. 2A). In rats carrying liver metastases, the radioactivity distribution in liver was heterogeneous, but the mean uptake was similar to that in normal liver at this time point. The decrease in ^{76}Br concentration in blood during the following 2 days was reflected in the PET images of heart and normal liver. The ^{76}Br uptake in liver containing metastases also decreased, while a gradual accumulation in subcutaneous tumors was observed. On the second day after ^{76}Br-38S1 injection, the most prominent regions of uptake were subcutaneous tumors and liver metastases.

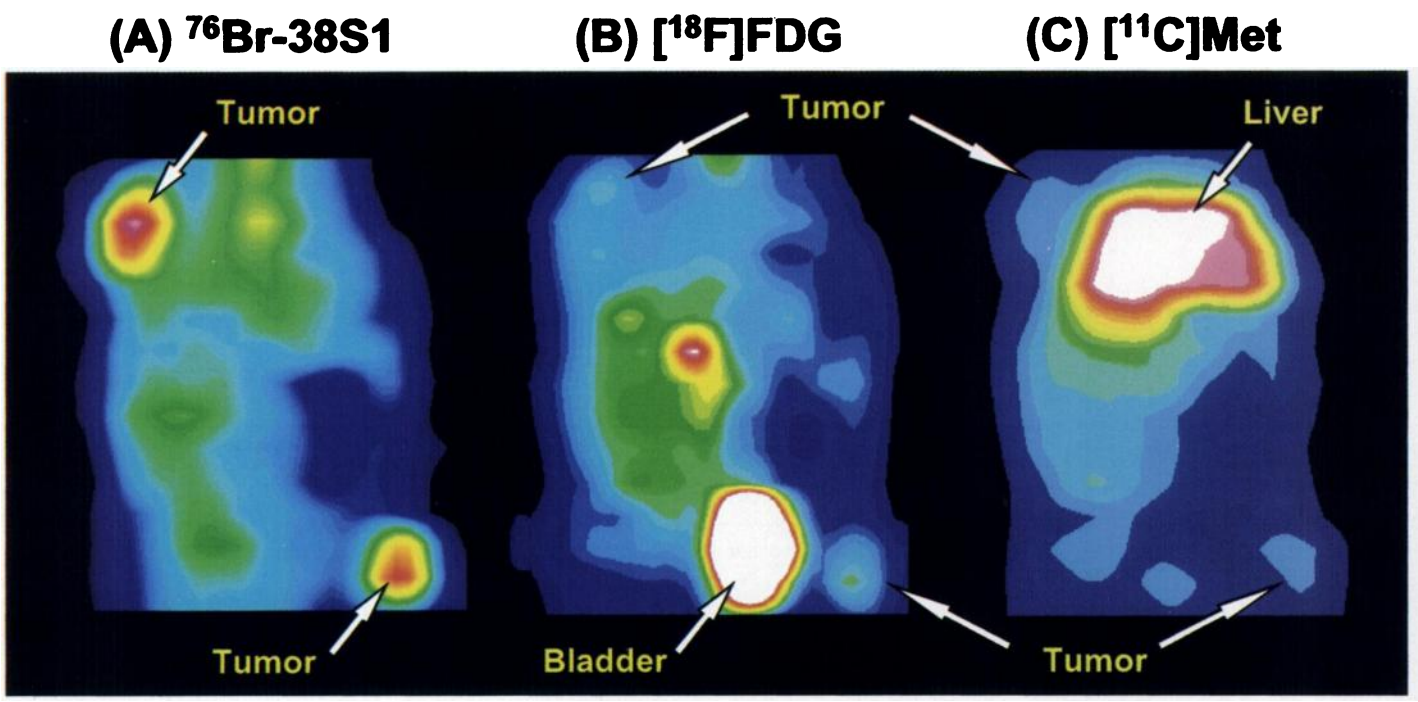

FIGURE 3. Coronally reconstructed PET images showing the distribution of ^{76}Br-38S1 (40 hr postinjection) (A), [^{18}F]FDG (30–48 min postinjection) (B) and [^{11}C]Met (16–45 min postinjection) (C) in the same rat carrying subcutaneous LS174T xenografts.

After injection of [^{18}F]FDG, the initially high uptake in the heart region, reflecting blood radioactivity, decreased rapidly in most rats to an almost constant level (Fig. 2B). However, after the first few minutes, the heart uptake in three rats increased continuously, to SUVs of 3.7 ± 0.6 (not included in Fig. 2B). This difference could be ascribed to different nutritional status affecting the glucose consumption of the heart (*28*). The kinetics of [^{18}F]FDG uptake in liver metastases differed from that of normal liver, in which the maximum uptake was reached around 2–3 min postinjection. Fluorine-18 activity in liver metastases increased steadily. A slow accumulation of ^{18}F activity was also observed in subcutaneous tumors but remained low in comparison with most normal tissues. The pharmacokinetics of [^{11}C]Met was characterized by a rapid washout from the heart region and a similar rapid uptake in liver (Fig. 2C). The SUVs obtained from measurements at the sites of subcutaneous tumors remained low in comparison with liver uptake.

PET Imaging

Figure 3 displays PET images of the distribution of ^{76}Br-38S1 (A), [^{18}F]FDG (B) and [^{11}C]Met (C) in the same rat carrying subcutaneous LS174T tumors in the right hindleg and left flank. Imaging of all three tracers was performed separately during a period of 6 hr (Fig. 1). Two days after administration of ^{76}Br-38S1, both tumor sites could be easily identified in the images, showing no other region of comparable uptake. The most prominent region of ^{18}F uptake in most rats was the bladder due to the rapid excretion of [^{18}F]FDG into urine. Prominent uptake was seen in the abdominal region, probably corresponding to the intestines. The tumor sites were barely distinguishable, which was also the case in the [^{11}C]Met images, where the dominant feature was, as expected, the intense accumulation of ^{11}C activity in the liver.

Figure 4 displays the PET images obtained after administration of ^{76}Br-38S1 (A) and [^{18}F]FDG (B) to a rat carrying numerous liver metastases of LS174T cells. Imaging of radiotracer distributions was performed over a period of 3 hr, in the case of ^{76}Br-38S1, 2 days after tracer administration. An increased uptake in the liver region in comparison with normal tissues could be observed for both radiotracers, and for [^{18}F]FDG, ^{18}F activity was also found in the intestinal region.

Whole-Body Autoradiography

Whole-body images of radioactivity distribution after injection of ^{76}Br-38S1, [^{18}F]FDG and [^{14}C]Met in the same rat are shown in Figure 5. In the subcutaneous flank tumor, the ^{76}Br activity 2 days after injection was found peripherally, surrounding necrotic regions of the tumor (Fig. 5A). By contrast, the tumor in the hindleg, with a rather intramuscular location in this animal, was characterized by several foci of high ^{76}Br accumulation in viable tumor tissue. Of the normal tissues, a uniform distribution of ^{76}Br was noted in liver and lungs, and in this rat, a region in the left part of the abdomen. The distribution of ^{18}F activity in the flank tumor was also peripheral (Fig. 5B). However, at the intramuscular tumor site, the ^{18}F uptake was, in contrast to ^{76}Br-activity, lower at this tumor site and located along the periphery of the tumor masses. Selective accumulation of [^{18}F]FDG could be observed in segments of the intestines and in the brain. Tumor distribution of [^{14}C]Met was

FIGURE 4. Coronally reconstructed PET images after the administration of ^{76}Br-38S1 (47 hr postinjection) (A) and [^{18}F]FDG (30–48 min postinjection) (B) to the same rat carrying liver metastases of LS174T cells.

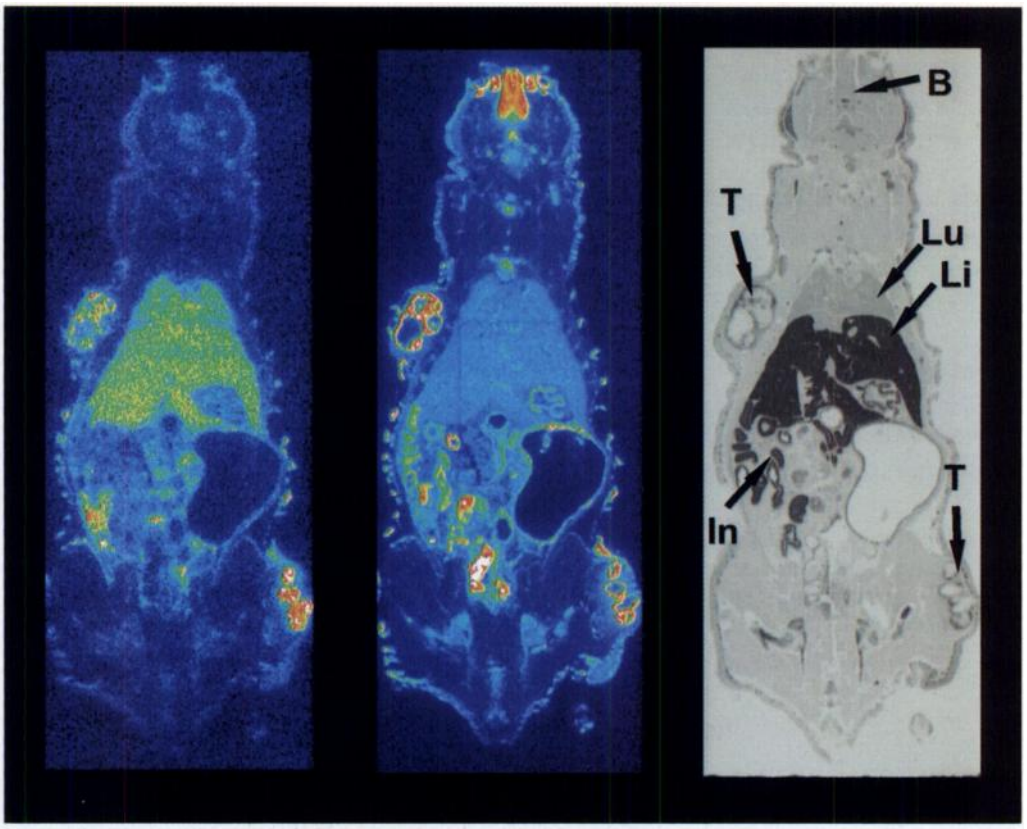

FIGURE 5. Whole-body autoradiograms after the administration of ^{76}Br-38S1 (47 hr postinjection) (A), [^{18}F]FDG (1 hr postinjection) (B) and [^{14}C]Met (1 hr postinjection) (C) in the same or adjacent slices. T = tumor; B = brain; In = intestine; Li = liver; Lu = lung.

similar to that of [^{18}F]FDG, although tumor uptake of ^{14}C activity was by far surpassed by its accumulation in liver and intestines (Fig. 5C).

Tumor-to-tissue ratios based on measurements of whole-body autoradiograms are shown in Table 1. Except for blood, liver and lungs, the ratio of tumor-to-normal organ uptake was higher for ^{76}Br-38S1 than for [^{18}F]FDG. Carbon-11-Met had the lowest ratios, except in the blood, intestines and brain.

Tissue Uptake

AIs of radioactivity after ^{76}Br-38S1, [^{18}F]FDG and [^{11}C]Met administration were calculated from measurements of dissected tumors and normal tissues in well scintillation gamma detectors, and selected results are presented in Figure 6. At 49 hr after injection of ^{76}Br-38S1, the highest ^{76}Br concentration was found in tumors (weighing 1.2 ± 0.7 g and 1.1 ± 0.2 g, for subcutaneous tumors and liver metastases, respectively). The highest uptake in normal tissues, apart from blood, was found in lungs. Although the variations in urine excretion and heart uptake of ^{18}F activity were considerable, the average AI of urine was the highest (12 ± 8), followed by heart (10 ± 7). The mean [^{18}F]FDG accumulations 1 hr postinjection in subcutaneous tumors and liver metastases (tumor masses of 0.5 ± 0.4 g and 0.9 ± 0.3 g, respectively) were similar at about 4, i.e., slightly higher than AI in brain (3.8 ± 2.1) and large intestine

TABLE 1
Tumor-to-Tissue Ratios in Whole-Body Autoradiograms from Two Rats Carrying Subcutaneous LS174T Xenografts

Tissue	^{76}Br-38S1	[^{18}F]FDG	[^{14}C]Met
Blood	1.2 (0.5)	3.2 (0.4)	1.5 (0.6)
Kidney	2.6 (1.8)	1.4 (0.4)	1.1 (0.2)
Spleen	7.1 (5.3)	3.2 (1.0)	1.8 (1.3)
Liver	1.3 (0.5)	2.6 (1.0)	0.3 (0.2)
Stomach	3.0 (0.9)	2.6 (1.3)	0.8 (0.3)
Small intestine	3.1 (0.7)	0.3 (0.2)	0.5 (0.2)
Lung	1.7 (0.8)	2.6 (1.0)	1.4 (0.5)
Muscle	22 (11)	15 (5.2)	1.8 (0.7)
Bone	6.3 (2.2)	3.1 (0.7)	0.7 (0.3)
Brain	17 (9)	1.1 (0.8)	2.1 (1.0)

Both rats had been injected with ^{76}Br-38S1 47 hr before sacrifice and a mixture of [^{18}F]FDG and [^{14}C]Met 1 hr before sacrifice. Data presented are means (s.d.) of measurements in 3–21 autoradiograms.

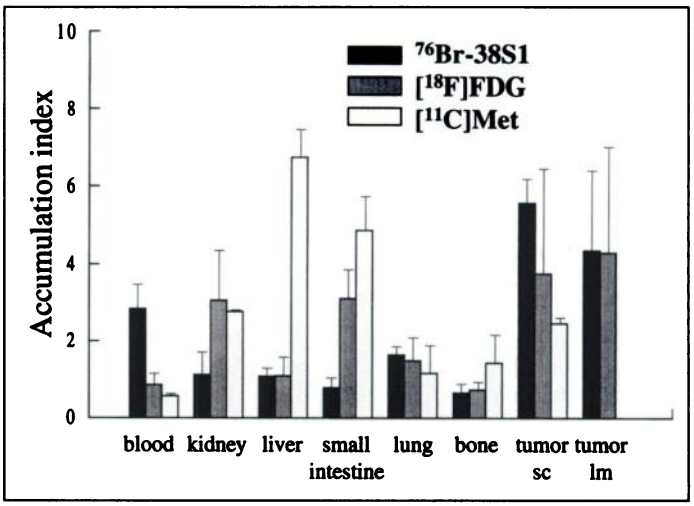

FIGURE 6. Tumor and tissue uptake of ^{76}Br-38S1 (solid bar, four animals) 2 days postinjection, [^{18}F]FDG (striped bar, five animals) 1 hr postinjection and [^{11}C]Met (open bar, two animals) 1 hr postinjection, measured by gamma counting. For tumors, each bar represents at least four specimens.

TABLE 2
Tumor-to-Tissue Values After Dissection of Rats Carrying Subcutaneous LS174T Xenografts or Liver Metastases Two Days After Administration of ^{76}Br-38S1 and 1 Hour After Injection of [^{18}F]FDG and [^{11}C]Met

	Subcutaneous tumors			Liver metastases	
Tissue	^{76}Br-38S1	[^{18}F]FDG	[^{11}C]Met	^{76}Br-38S1	[^{18}F]FDG*
Blood	1.7 (0.2)	5.3 (3.3)	4.4 (1.4)	1.8 (0.6)	4.1 (2.8)
Kidney	7.7 (2.0)	1.0 (0.6)	0.9 (0.3)	2.8 (0.7)	1.8 (1.4)
Spleen	5.8 (1.3)	3.0 (2.1)	1.3 (0.5)	3.4 (1.0)	2.5 (1.5)
Liver	5.4 (1.4)	4.7 (2.7)	0.4 (0.2)	4.1 (2.0)	3.5 (2.3)
Stomach	7.6 (0.8)	2.2 (1.3)	0.8 (0.3)	2.6 (1.0)	2.0 (1.3)
Small intestine	9.1 (1.0)	1.2 (0.9)	0.5 (0.2)	4.4 (1.2)	1.3 (0.9)
Lung	3.3 (0.5)	2.1 (1.3)	2.0 (0.7)	2.8 (0.9)	3.3 (2.1)
Muscle	14 (3.2)	12 (8)	4.8 (1.5)	6.4 (1.2)	17 (12)
Bone	11 (3)	4.1 (3.0)	1.8 (0.6)	5.4 (1.4)	6.8 (4.5)
Brain	32 (4)	1.4 (1.0)	4.3 (1.3)	11 (4)	0.8 (0.6)

Data presented are means (maximum errors) of samples from two animals.
*Samples from three animals were analyzed.

(3.4 ± 1.2). The highest accumulation of [^{11}C]Met was found in abdominal organs, including liver, pancreas (6.5 ± 0.5) and small intestine. The concentration of [^{11}C]Met was only studied in rats carrying subcutaneous tumors, weighing 0.8 ± 0.3 g.

Tumor-to-tissue ratios were calculated for each rat and tumor (Table 2). In comparison with the other tracers, ^{76}Br-38S1 had, regarding subcutaneous LS174T tumors, higher tumor-to-tissue ratios except for blood. The ^{76}Br uptake in tumors vis-à-vis normal tissues was, in most cases, lower for liver metastases than for subcutaneous tumors, whereas [^{18}F]FDG ratios generally were of the same order for both tumor models. This resulted in better metastases-to-tissue ratios regarding blood, lungs, muscle and bone for [^{18}F]FDG than ^{76}Br-38S1.

DISCUSSION

In the current study, the experimental tumor-imaging qualities of the ^{76}Br-labeled anti-CEA MAb 38S1 were compared with those of the two most commonly applied PET tracers for tumor detection, [^{18}F]FDG and [^{11}C]Met. The uptake of ^{76}Br-38S1 in the animal models was found to be more selectively restricted to tumor tissue than that of the other two tracers, for which high accumulation was found in the liver ([^{11}C]Met), urinary system ([^{18}F]FDG) and segments of the intestines (both). This pattern of normal tissue uptake of [^{18}F]FDG has also been observed in humans (*29*). The disadvantage of using ^{76}Br-labeled 38S1 was the considerable ^{76}Br activity still found in the blood 2 days after administration, at which time the tumor uptake was maximum in a previous experimental study of the ^{76}Br-38S1 kinetics (*21*). The blood clearance of intact MAbs is slow, and dehalogenation of a ^{76}Br-labeled MAb may result in a substantial amount of free radiobromide in the extracellular space (*21*). Although this causes a higher normal tissue background of radioactivity in organs containing a large extracellular space or a large blood pool such as the liver, the presence of liver metastases could be verified by PET imaging using ^{76}Br-38S1.

Identification of liver metastases was also possible by [^{18}F]FDG imaging, not only by a relatively high radiotracer uptake but also by a distinctly different kinetic pattern than that of normal liver. This is one example of how the kinetic information obtained in the PET investigation could give additional information to facilitate the identification of malignant lesions. Although the average [^{18}F]FDG accumulation in dissected liver metastases was not significantly higher than that in subcutaneous tumors, PET imaging of the subcutaneous tumor type was less successful when [^{18}F]FDG rather than ^{76}Br-38S1 was used. Fluorine-18-FDG has been shown to accumulate to a lesser degree in subcutaneous tumors from colorectal cancer than in xenografts from several other tumor types (*30*).

An interesting observation was that certain tumor regions both in PET images and in autoradiograms exhibited a high ^{76}Br activity yet failed to show a corresponding high ^{18}F uptake, and vice versa. Because [^{18}F]FDG is presumed to accumulate mainly in metabolically active cells, a high uptake of MAb could be partly explained by CEA expression of quiescent cells with a low [^{18}F]FDG uptake. Some investigators have also found that antibodies may to some extent be located in necrotic regions, possibly related to the presence of antigen in these areas (*31*). However, in the case of MAb 38S1, this was contradicted by findings in previous studies on the microscopical tumor distribution, where no antibody accumulation in necrotic areas could be found (*32*). The more pronounced [^{18}F]FDG uptake than ^{76}Br-38S1 uptake in some tumor areas most probably reflects the slower diffusion of high-molecular weight antibodies through tumor tissue (*33*).

Carbon-11-Met was only studied in the subcutaneous tumor model because, due to its high accumulation in liver, this tracer does not readily lend itself to imaging of liver metastases. In the subcutaneous tumor model, the tumor uptake in relation to normal organs was the lowest of the three tracers applied, and tumor sites were barely visualized by PET. As expected, the histopathological tumor distribution of [^{14}C]Met was similar to that of [^{18}F]FDG.

In PET images, measurements of objects with a size comparable to, or smaller than, the PET resolution will underestimate the radioactivity concentration (*34*). With small experimental animals such as rats, an underestimation of radioactivity uptake in most experimental tumors and essentially all organs except liver may be expected. The radioactivity concentration could therefore be identical in two tumors, yet appear to differ in the PET images due to differences in tumor size. The present investigation was designed to allow PET imaging of all three radiotracers in some animals, thereby minimizing the possibility of misinterpreting images due to different sizes of the objects studied.

For absolute quantification of tracer biodistribution in small animals, methods such as measuring radioactivity concentration in dissected tissues after exsanguination are commonly applied. However, the extrapolating of such data to the in vivo situation may be misleading in the case of radiolabeled compounds with a high concentration in blood, such as antibodies. For instance, although the average metastases-to-liver ratios for dissected tissues were higher for ^{76}Br-MAb than for [^{18}F]FDG, the corresponding in vivo ratios probably change in favor of the latter tracer.

Whole-body autoradiography is an effective means to visualize tissue distribution of radioactivity without removal of blood. Indeed, the tumor-to-tissue ratios for ^{76}Br-38S1 were in some cases, e.g., liver, considerably lower when using data obtained by this method than by gamma counting of dissected samples. For [^{18}F]FDG and [^{11}C]/[^{14}C]Met, the differences in tumor-to-tissue ratios evaluated by the two techniques were less pronounced, consistent with their low concentration in blood. The higher resolution of whole-body autoradiography provides detailed regional information about the tracer distribution within each tumor and organ. This is of particular advantage in

the case of tumors because tumors, and therefore their distribution patterns of radiotracers, are heterogeneous.

CONCLUSION

PET imaging of human colonic cancer xenografts using a ^{76}Br-labeled anti-CEA antibody proved feasible and, in these models, superior in several respects to tumor imaging with [^{18}F]FDG and [^{11}C]Met. Applying different techniques for the evaluation of tracer distribution, PET, whole-body autoradiography and gamma counting of dissected tissues, provided useful information for the comparison of the tumor imaging agents. For instance, although the uptake of ^{76}Br-38S1 in dissected normal tissues was low, whole-body autoradiography revealed that the relatively high blood content of ^{76}Br activity resulted in an overall higher background radioactivity, which decreased tumor-to-tissue ratios. Affecting both tumor contrast and normal organ dosimetry, the blood background of slowly clearing radiotracers is an important consideration in animal studies. Another observation made both by PET imaging and autoradiography was that the tumor accumulation of [^{18}F]FDG and the ^{76}Br-labeled antibody differed, in some aspects, both quantitatively and qualitatively. Provided that such information could be correctly interpreted, multitracer PET imaging, applying metabolical tracers as well as MAbs directed against tumor antigens of biological importance (*35*), might give additional knowledge about each malignant lesion and therefore influence the choice of therapy.

ACKNOWLEDGMENTS

We thank Mrs. Veronica Asplund and the staff members of the Uppsala University PET Center and the Svedberg Laboratory for valuable technical assistance. This work was supported by the Swedish Cancer Society, Grants 2971-B92-03XAA and 1176-B94-03TAA, and the Swedish Medical Research Council, Grant B94-39X-10888-01A.

REFERENCES

1. Warburg O. *The metabolism of tumors*. London: Constable; 1930.
2. Strauss LG, Scott PS. The applications of PET in clinical oncology. *J Nucl Med* 1991;32:623–648.
3. Messa C, Choi Y, Hoh CK, et al. Quantification of glucose utilization in liver metastases: parametric imaging of FDG uptake with PET. *J Comput Assist Tomogr* 1992;16:684–689.
4. Yonekura Y, Benua RS, Brill AB, et al. Increased accumulation of 2-deoxy-2-[^{18}F]fluoro-D-glucose in liver metastases from colon carcinoma. *J Nucl Med* 1982; 23:1133–1137.
5. Ito K, Kato T, Tadokoro M, Ishiguchi T, Oshima M, Ishigaki T, Sakuma S. Recurrent rectal cancer and scar: differentiation with PET and MR imaging. *Radiology* 1992; 182:549–552.
6. Strauss LG, Clorius JH, Schlag P, et al. Recurrence of colorectal tumors: PET evaluation. *Radiology* 1989;170:329–332.
7. Lilja A, Bergström K, Hartvig P, Spännare B, Halldin C, Lundqvist H, Långström B. Dynamic study of supratentorial gliomas with L-methyl-^{11}C-methionine and positron emission tomography. *Am J Neuroradiol* 1985;6:505–514.
8. Bergström M, Muhr C, Lundberg PO, et al. Amino acid distribution and metabolism in pituitary adenomas using positron emission tomography with D-[^{11}C]methionine and L-[^{11}C]methionine. *J Comput Assist Tomogr* 1987;11:384–389.
9. Fujiwara T, Matsuzawa T, Kubota K, et al. Relationship between histologic type of primary lung cancer and carbon-11-L-methionine uptake with positron emission tomography. *J Nucl Med* 1989;30:33–37.
10. Kubota K, Matsuzawa T, Masatoshi I, et al. Lung tumor imaging by positron emission tomography using carbon-11-L-methionine. *J Nucl Med* 1985;26:37–42.
11. Larson SM, Pentlow KS, Volkow ND, et al. PET scanning of iodine-124–3F9 as an approach to tumor dosimetry during treatment planning for radioimmunotherapy in a child with neuroblastoma. *J Nucl Med* 1992;33:2020–2023.
12. Philpott GW, Schwarz SW, Anderson CJ, et al. RadioimmunoPET. Detection of colorectal carcinoma with positron-emitting copper-64-labeled monoclonal antibody. *J Nucl Med* 1995;36:1818–1824.
13. Wilson CB, Snook DE, Dhokia B, et al. Quantitative measurement of monoclonal antibody distribution and blood flow using positron emission tomography and ^{124}iodine in patients with breast cancer. *Int J Cancer* 1991;47:344–347.
14. Goldenberg DM, Larson SM. Radioimmunodetection in cancer identification. *J Nucl Med* 1992;33:803–814.
15. Larson SM. Clinical radioimmunodetection 1978–1988: overview and suggestions for standardization of clinical trials. *Cancer Res* 1989;5(suppl):892–898.
16. Collier DB, Abdel-Nabi H, Doerr RJ, et al. Immunoscintigraphy performed with In-111-labeled CYT-103 in the management of colorectal cancer: Comparison with CT. *Radiology* 1992;185:179–186.
17. Haseman MK, Brown DW, Keeling CA, Reed NL. Radioimmunodetection of occult carcinoembryonic antigen-producing cancer. *J Nucl Med* 1992;33:1750–1757.
18. Lind P, Lechner P, Arian Schad K, Klimpfinger M, Cesnik H, Kammerhuber F, Eber O. Anti-carcinoembryonic antigen immunoscintigraphy (Tc-99m-monoclonal antibody BW4321/26) and serum CEA levels in patients with suspected primary and recurrent colorectal carcinoma. *J Nucl Med* 1991;32:1319–1325.
19. Markowitz A, Saleemi K, Freeman LM. Role of In-111-labeled CYT-103 immunoscintigraphy in the evaluation of patients with recurrent colorectal carcinoma. *Clin Nucl Med* 1993;18:685–700.
20. Lövqvist A, Sundin A, Ahlström H, Carlsson J, Lundqvist H. ^{76}Br-labeled monoclonal anti-CEA antibodies for radioimmuno positron emission tomography. *Nucl Med Biol* 1995;22:125–131.
21. Lövqvist A, Sundin A, Ahlström H, Carlsson J, Lundqvist H. Pharmacokinetics and experimental PET imaging of a 76Br-labeled monoclonal anti-CEA antibody. *J Nucl Med* 1997;38:395–401.
22. Scott-Robson S, Capala J, Malmborg P, Lundqvist H. Production of ^{76}Br and its use in labeling proteins. *Acta Radiol* 1991;376(suppl):64.
23. Hedin A, Hammarström S, Larsson Å. Specificities and binding properties of eight monoclonal antibodies against carcinoembryonic antigen. *Mol Immunol* 1982;19: 1641–1648.
24. Toorongian SA, Mulholland GK, Jewett DM, Bachelor MA, Kilbourn MR. Routine production of 2-deoxy-2-[^{18}F]fluoro-D-glucose by direct nucleophilic exchange on a quaternary 4-aminopyridinium resin. *Nucl Med Biol* 1990;17:273–280.
25. Långström B, Antoni G, Gullberg P, et al. Synthesis of L- and D-[methyl-^{11}C]methionine. *J Nucl Med* 1987;28:1037–1040.
26. Graf W, Sundin A, Glimelius B, Ahlström H, Carlsson J. Induction and quantification of hepatic metastases from a human colonic cancer in the nude rat. *Eur J Surg Oncol* 1992;18:608–614.
27. Ullberg S, Larsson B, Tjälve H. Autoradiography. In: Glenn HJ, ed. *Biologic applications of radiotracers*. Boca Raton, FL: CRC Press, 1982:56–108.
28. Yamada K, Endo S, Fukuda H, et al. Experimental studies on myocardial glucose metabolism of rats with ^{18}F-2-fluoro-2-deoxy-D-glucose. *Eur J Nucl Med* 1985;10: 341–345.
29. Hoh CK, Hawkins RA, Glaspy JA, et al. Cancer detection with whole-body PET using 2-[^{18}F]fluoro-2-deoxy-D-glucose. *J Comput Assist Tomogr* 1993;17:582–589.
30. Wahl RL, Hutchins GD, Buchsbaum DJ, Liebert M, Grossman HB, Fischer S. ^{18}F-2-deoxy-2-fluoro-D-glucose uptake into human tumor xenografts. *Cancer* 1991; 67:1544–1550.
31. Brown RS, Fisher SJ, Wahl RL. Autoradiographic evaluation of the intratumoral distribution of 2-deoxy-D-glucose and monoclonal antibodies in xenografts of human ovarian adenocarcinoma. *J Nucl Med* 1993;34:75–82.
32. Ahlström H, Carlsson L, Hedin A, Lörelius LE. The spatial distribution of parentally administered monoclonal antibodies against CEA in a human colorectal tumor xenograft. *Acta Oncol* 1989;28:81–86.
33. Jain RK. Physiological barriers to delivery of monoclonal antibodies and other macromolecules in tumors. *Cancer Res* 1990;50(suppl):814–819.
34. Litton JE, Bergström M, Eriksson L, Bohm C, Blomqvist G, Kesselberg M. Performance study of the PC-384 positron camera system for emission tomography of the brain. *J Comput Assist Tomogr* 1983;8:74–87.
35. Larson SM, Macapinlac HA, Scott AM, Divgi CR. Recent achievements in the development of radiolabeled monoclonal antibodies for diagnosis, therapy and biologic characterization of human tumors. *Acta Oncol* 1993;32:709–715.